13th World Conference on Earthquake Engineering
Vancouver, B.C., Canada
August 1-6, 2004
Paper No. 2105

DEVELOPMENT OF STRENGTHENING METHOD USING ATTACHED BRACES IN OUTER FRAME

Tsunehisa MATSUURA[1], Kazuyuki SUMI[2] and Toshirou MAKITA[3]

SUMMARY

A new seismic strengthening method using outer-frame braces is proposed. The braces are attached outside the structural frames of existing buildings and linked via newly added reinforced concrete beams. This method involves uncomplicated works to achieve highly-effective resistance against severe earthquakes. Shear force during an earthquake is transferred from the existing structure to the braces through connecting beams. Therefore, accurate evaluation of connecting beam performance is essential. Based on 1/3-scale specimens, four reinforced concrete frames were tested under lateral loads. The test variables were: with/without the attached brace and failure mode of the frame. This paper describes the performance of the reinforced concrete frames strengthened by using attached braces, and evaluation of the resultant strength of the frame.

INTRODUCTION

The 1995 Hyogoken Nanbu Earthquake exposed the seismic vulnerability of reinforced concrete buildings designed in accordance with pre-1980 design methods. A large number of these buildings still exist, and would be severely damaged in a major earthquake. Strengthening measures should be carried out immediately. During repair and strengthening works, if a building were strengthened by adding reinforced concrete walls or a steel frame with braces, the element of seismic structure would be close to the doorways or windows. Moreover, those methods have a negative effect on indoor lighting. It is difficult to occupy a building under construction; therefore, repair work should be completed within a short time. A new seismic strengthening method that can be carried out easily without decreasing the serviceability of the building is required.

A new seismic strengthening method was developed using outer-frame braces, as shown in Fig. 1. This method is highly effective in resisting severe earthquakes, increasing the strength of the building by attaching outer-frame tension braces. Braces are placed outside the structural frame of existing buildings and linked via newly added reinforced concrete beams. The developed method has the following

[1] Technical Research Institute, HAZAMA Corp., Japan, email:matsuura@hazama.co.jp
[2] Design and Technical Center, HAZAMA Corp., Japan, email:sumi@hazama.co.jp
[3] Design and Technical Center, HAZAMA Corp., Japan, email: makita@hazama.co.jp

characteristics: The work time in each room is short, and the strengthening procedure is easy. Moreover, serviceability of building is not reduced.

The strengthening procedure is described below. First, the connecting beam was cast on the existing frame. Second, the anchorage device was jointed to the connecting beam. Last, the braces were tied to the anchorage device with pin joints at both ends. The existing building, connecting beam and anchorage device were joined under normal stress conditions by pulling the prestressing bars.

RESEARCH SIGNIFICANCE

If the buildings designed in accordance with pre-1980 design methods were to experience a major earthquake, they would be severely damaged. It is necessary to increase the seismic performance to decrease damage to these buildings.

This study presents an investigation on the performance of strengthened reinforced concrete frames following the implementation of a simple strengthening method using outer-frame braces. Two types of loading tests for the connection beams and reinforced concrete frames were conducted. The experiment confirmed the load-deflection curves of the connecting reinforced concrete beam, and the performance and lateral load-carrying capacity of the strengthened reinforced concrete frames.
A comprehensive design procedure for strengthening reinforced concrete frames by attaching outer-frame braces is proposed.

This paper describes the performance of the reinforced concrete frames strengthened using the attached braces, and evaluation of the resultant strength of frames.

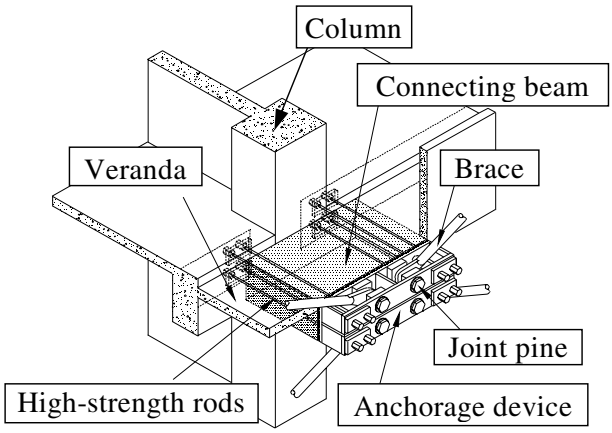

Fig. 1. Outline of strengthening method

EXPERIMENTAL PROGRAM

Specimen Details and Material

A 1/3-scale test was arranged in order to study the behavior of the strengthened reinforced concrete frames using attached braces. The specimens are shown in Table 1, and details of the original and connecting beams are shown in Fig. 2. The test variables were: failure mode of columns and with/without attached braces. Four specimens were tested: No. 1 is an original RC frame with columns designed to fail in shear. No. 2 is strengthened No. 1 using an attached brace. No. 3 is an original RC frame with columns designed to fail in flexure. No. 4 is strengthened No. 3 using an attached brace. The bar arrangement of the beams was designed on all specimens so as to ensure that the beams would not fail in flexure or shear before the column failed.

The dimensions of the specimens are 2000 mm (span) × 1000 mm (story height). The cross sections of the column and beam elements are 250 × 250 mm and 180 × 250 mm, respectively. The beam has a slab 50 mm thick and 415 mm wide on both sides. For No. 1 and No. 2, the columns were reinforced with 12 deformed D13 (diameter = 13 mm, yield stress = 390 MPa) bars distributed evenly around the perimeter of the column cross section. Round Φ-4 (diameter = 4 mm, yield stress = 445 MPa) hoops spaced at 150 mm intervals were used as transverse reinforcement. For No. 3 and No. 4, the columns were reinforced with 12 deformed D10 (diameter = 10 mm, yield stress = 351 MPa) bars distributed evenly around the perimeter of the column cross section. Round Φ-4 hoops spaced at 35 mm intervals were used as transverse reinforcement. The bar arrangement of the beam is common in all specimens. The top and bottom reinforcement for the beams were taken to be 3 deformed D19 (diameter = 19 mm, yield stress = 360 MPa) bars, respectively. Deformed D6 (diameter = 6 mm, yield stress = 394 MPa) stirrups spaced at 100 mm intervals were used as transverse reinforcement.

The connecting beam element is such that the cross section is 500 × 170 mm, the longitudinal bars consist of 4 high-strength rods Φ-13 (yield stress = 1249 MPa), and 8 normal-strength deformed D13 (yield stress = 342 MPa) bars. Two deformed D6 stirrups spaced at 64 mm intervals were used as transverse reinforcement. The brace rod, 25 mm in diameter, has a yield strength of 295 MPa.

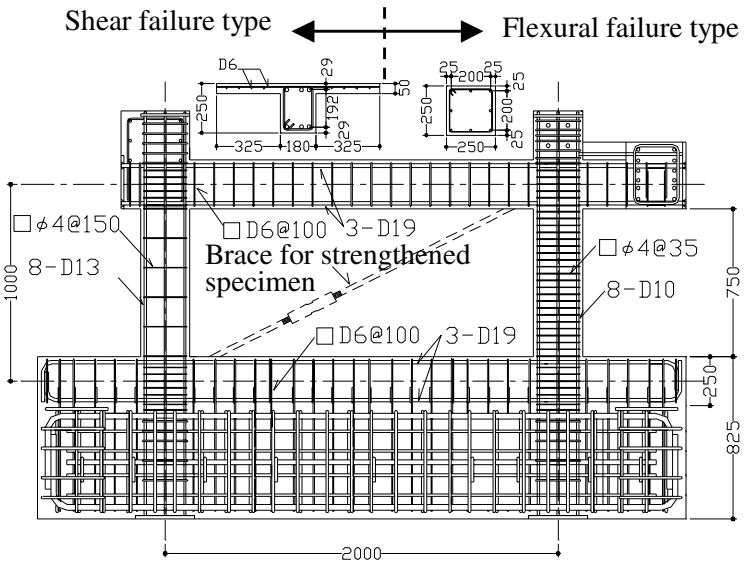

(a) Original frame

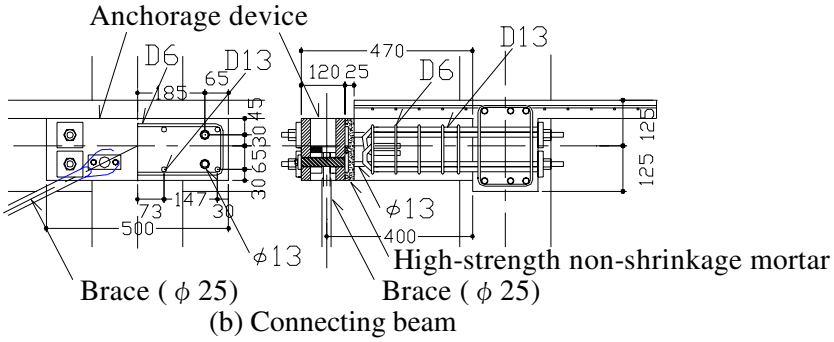

(b) Connecting beam

Fig. 2. Details of experimental specimen (Unit : mm)

Each specimen was cast in three stages: first the base stub, then the lower beam, and finally the columns and upper beam. The strengthening procedure was carried out through the following steps: (a) The rods and winding sheaths were inserted under the part where the connecting beam was cast beforehand; (b) The concrete surface of the area under the connecting beam was roughened; (c) The connecting beam was cast; (d) The anchorage device was jointed to the connecting beam with a clearance space of 2.5 cm between; (e) High-strength non-contraction mortar was used to fill the clearance space between the connection beam and anchorage device. After the mortar hardened, the prestressing bars were pulled and normal stress of 2.5 MPa was applied to the joint surface. Cement slurry was injected into the winding sheaths under pressure; (f) The braces were tied to the anchorage device with pin joints at both ends.

The concrete used for the columns and beams consisted of coarse aggregate with a maximum size of 15 mm. That of the connecting beams was 20 mm.

Table 1. Details of specimens

Specimen		No.1	No.2	No.3	No.4
Failure Mode		Shear failure	Shear failure	Flexural failure	Flexural failure
Attached Brace		without	With	without	with
Concrete Strength (MPa)	Column, Beam	24.6	25.5	25.6	29.5
	Connecting beam	-	40.3	-	37.8

Testing Procedure and Instrumentation

The experimental system is shown in Fig. 3. The test setup was designed to subject the test frame to cyclic lateral forces in one direction, while the axial load remained constant. Using prestressing rods, the bottom stub was securely tied to the strong floor, while the top end of columns were free to slide without inducing any rotation, thereby simulating the conditions in a rigid floor. Axial load was applied at $0.15\sigma_B \times B \times D$. In this experimental investigation, the applied lateral load was controlled by increments. The lateral load was created by 2 oil jacks connected to a loading stub on both sides. During testing, the oil jacks were controlled at the same load.

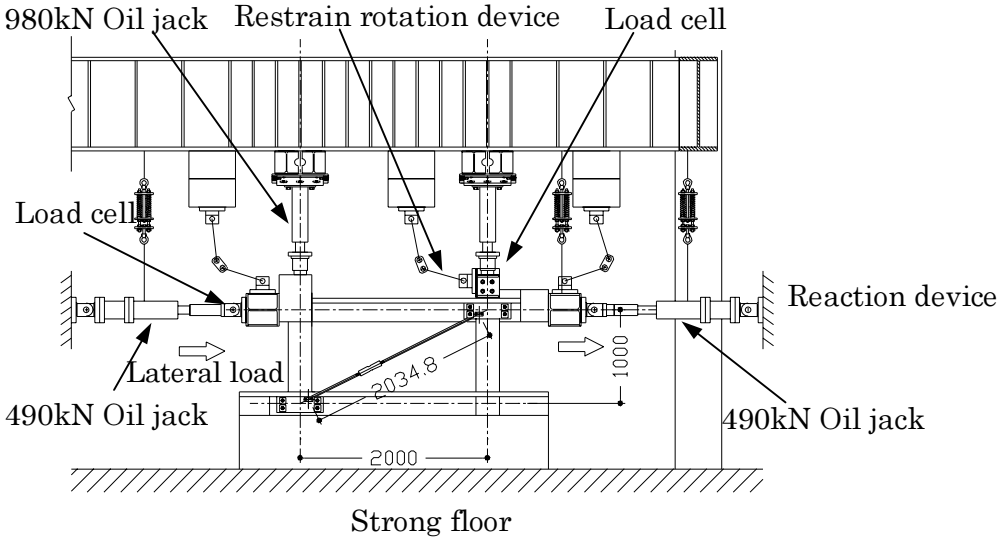

Fig. 3. Experimental set-up

Lateral load and axial load were measured using load cells placed with each jack. Displacement of columns in the horizontal and vertical direction, and displacement of the frame in the diagonal direction were measured and recorded electronically. Strain gauges were mounted to the column and beam reinforcement to measure column and beam strains. In addition, brace strains and displacement between anchorage devices were measured. Each displacement was measured using a linear variable displacement transducer (LVDT).

EXPERIMENTAL RESULTS

Visual and Measured Observations

Test results for all specimens are reported in Table 2. Figure 4 illustrates the lateral load-displacement behavior of each specimen. The horizontal displacement of the beam was divided by the height between the upper and lower beam centers to obtain the drift angle. All specimens showed severe damage to the columns during the final stage of the tests, and different crack patterns developed for each specimen. Figure 5 shows the crack patterns of all specimens in the compression side of the column.

First, the results for No. 1, the original shear failure specimen, are described. As the load was increased, flexural crack and flexural-shear crack were observed at the top and bottom column face on the compression side of the column, in succession. Shear crack was observed on the beam at drift angle of 0.6%. When displacement of the frame increased beyond a drift angle of about 0.75%, reinforcement at the bottom on the compression side of the column reached yield stress. It occurred continuously on the tension side. As the displacement increased to a drift angle of about 1.3%, the compression side of the column suddenly failed in shear immediately after the shear crack occurred, and the compression side lost its axial load-carrying capacity.

The results for No. 2, the strengthened shear failure specimen, are described. No. 2 has higher elastic stiffness than No. 1. As the load was increased, flexural cracks were observed at the top and bottom column faces on the compression side of the column, in succession. Shear crack was observed at the bottom on the compression side at a drift angle of 0.4%. There were fewer cracks on No. 2 than on No. 1. When displacement of the frame increased beyond a drift angle of about 0.6%, reinforcement at the bottom on the tension side of the column reached tension yield stress. Moreover, reinforcement at the bottom on the compression side of the column reached compression yield stress. In addition, shear crack was observed in the beam near the connecting beam joint. As the displacement increased to a drift angle of about 0.9%, the compression side of the column suddenly failed in shear immediately after the width of the shear crack on the compression side expanded, and the compression side lost its axial load-carrying capacity.

The results for No. 3, the original flexural failure specimen, are described. As the load was increased, flexural cracks were observed at the top and bottom column faces of the compression side of the column, in succession. At a drift angle of 0.3%, reinforcement at the bottom of both the tension and compression sides of the column reached tension yield stress, and shear crack was observed on the beam. When displacement of the frame increased beyond a drift angle of about 0.6 to 0.75%, reinforcement at the top of each column yielded in tension. Moreover, the stiffness on the load-displacement curve decreased. A small amount of concrete crushing occurred at the bottom of the compression column at a drift angle of 1.5%. At a drift angle of about 2.0%, the maximum lateral load was reached. At increased displacement, load-carrying capacity decreased gradually. After the concrete at the top of the compression side of the column was crushed at a drift angle of 3.5%, shear crack occurred on the compression side immediately, and the lateral load decreased abruptly. In addition, as displacement increased to a drift angle of 4.15%, the compression side of the column lost its axial load-carrying capacity.

Next, the results of No. 4, the strengthened flexural failure specimen, are described. No. 4 has higher elastic stiffness than No. 3. No. 4 had nearly the same flexural crack pattern of No. 3. At a drift angle of 0.4%, reinforcement at the bottom of both the tension and compression sides of the column reached tension yield stress. Shear crack was observed on the compression side at a drift angle of 0.65%. When displacement of the frame increased beyond a drift angle of about 0.7 to 1.0%, reinforcement at the top of each column yielded in tension. Moreover, the stiffness on the load-displacement curve decreased. At a drift angle of 1.2%, strain of the brace reached yield strain. At a drift angle of about 1.5%, concrete crushing occurred at the top and bottom of the compression side of the column, and the maximum lateral load was reached. In the second cycle of loading at a drift angle of 1.5%, concrete crushing developed, and the load-carrying capacity decreased. At a drift angle of 1.64%, the compression side of the column suddenly failed in shear immediately after the width of shear crack expanded, and the compression side of the column lost its axial load-carrying capacity.

Table 2. Test results

Specimen	Maximum Load		Ultimate State*	Brace Yield	
	Shear Force (kN)	Drift Angle (%)	Drift Angle (%)	Shear Force (kN)	Drift Angle (%)
No.1	397.6	1.35	1.35	–	–
No.2	405.5	0.92	0.92	405.3	0.91
No.3	267.1	1.95	4.15	–	–
No.4	421.1	1.47	1.64	390.6	0.87

*: Lost axial load carrying capacity

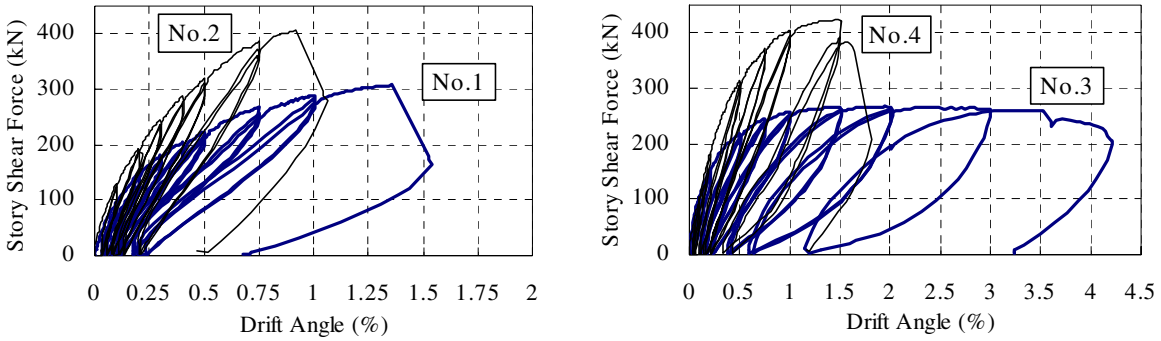

(a) Shear failure type (b) Flexural failure type

Fig. 4. Lateral load–displacement responses

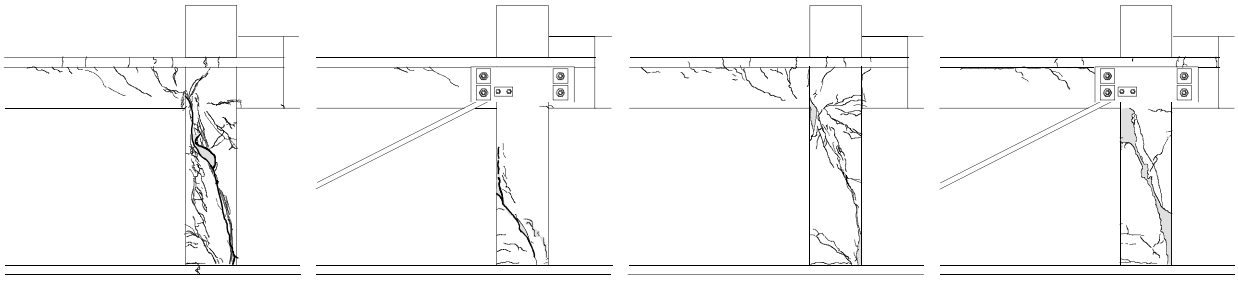

(a) No. 1 (b) No. 2 (c) No. 3 (d) No. 4

Fig. 5. Crack patterns

Evaluation of Experimental Data

Lateral Load-Carrying Capacity

The lateral load-displacement peak envelopes of each specimen are provided in Fig. 6. Herein, strengthened specimens No. 2 and No. 4 use the lateral load, subtracting the horizontal component of the axial load, which had been acting on the brace from the jack load measured with the load cells. The brace axial load was obtained by multiplying the section area, using Young's module, by the average strain of the brace. The distance between the upper and lower connecting beams was divided by the original length to obtain the average strain of the brace.

Original and strengthened specimens exhibited responses up to the lateral load-carrying capacity with very similar lateral load-displacement curves. This is seen in both shear and flexural failure type specimens. Lateral load-carrying capacity of the strengthened specimens can be estimated by adding the strength of the original frame to the brace strength.

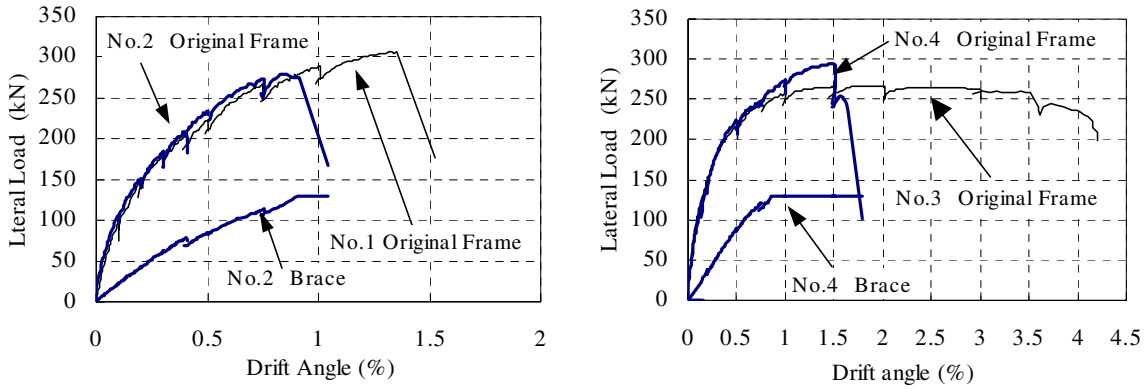

(a) Shear failure type (b) Flexural failure type

Fig. 6. Lateral load-displacement response

Deformation capacity

The lateral load-displacement peak envelopes of each specimen are provided in Fig. 6. The drift angle that had reached maximum load on the lateral load-displacement curve is 1.35% in No. 1 and 0.92% in No. 2. The compression side of the column of each specimen lost its axial load-carrying capacity immediately after the displacement reached the lateral load-displacement peak. The failure mode was shear failure, which was brittle on No. 1, and No. 2. Therefore, the deformation capacity of No. 2 was less than that of No.1.

Next, the results of the flexural failure series is described. The drift angle that had reached maximum load on the lateral load-displacement curve is 1.95% in No. 3 and 1.47% in No. 4. When each specimen lost its axial load-carrying capacity, the drift angle became 4.15% and 1.64%, respectively. The deformation capacity of No. 4 was less than that of No. 3. The reason for the large difference in the deformation capacity is believed to be as follows. After No. 3 exhibited ductility response to the load-displacement curve, shear crack occurred on the compression side of the column at a drift angle of 3.52%. However, No. 4 was observed to experience shear crack at a drift angle of 0.6% in an early stage. Before, No. 4 did not exhibit ductility response to the load-displacement curve, and the compression side of the column had failed in shear. For shear crack to occur, the rate of shear deformation to frame deformation had increased at a small deformation. As a result, when shear deformation reached ultimate deformation, the deformation capacity of No. 4 decreased more than No. 3.

Deformation capacity of the specimens was evaluated by column shear strength ratio using the JBDPA seismic evaluation standard [1]. This expression is obtained by dividing shear strength Q_{su} by flexural strength Q_{mu}, which are given by.

$$Q_{su} = \left\{ \frac{0.092 \cdot k_u \cdot k_p (18 + F_c)}{M/(Q \cdot d) + 0.12} + 0.85\sqrt{p_w \sigma_{wy}} + 0.1\sigma_0 \right\} \cdot b \cdot j \quad \text{(units: N, mm)} \quad (1)$$

$$Q_{mu} = 2[0.8 \cdot a_t \cdot \sigma_y D + 0.5ND(1 - \frac{N}{bDF_c})]/h_0 \quad (2)$$

Where k_u is the coefficient of size effect, k_p is the coefficient of tension reinforcement ratio, F_c is the concrete strength, M/(Q·d) is the shear span ratio, p_w is the transverse reinforcement ratio, σ_{wy} is the transverse reinforcement strength, σ_0 is the axial stress, b is the width, j is the distance between tension and compression resultants. a_t, σ_y, D, N, h_0 is the total sectional area of tension reinforcement, the strength of reinforcement, the depth, the axial force, and the clearance span of column, respectively.

When the shear strength and flexural strength were calculated, the axial load used was the value in which the shear force of the beam and the component of the vertical force of the brace were added to the constant axial load. The beam shear force was calculated in accordance with the following. Based on Bernoulli-Euler hypothesis, the end moment of the beam was calculated using the strain in the reinforcing bars. Next, the shear force was calculated by the end moment of both sides.

Table 3 presents the calculated results. Figure 7 shows the relationship between shear strength ratio and deformation capacity. The line in the figures indicates the ultimate drift angle calculated in accordance with the JBDPA seismic evaluation standard. All results of experimental deformation capacity were greater than those given by the JBDPA seismic evaluation standard. Deformation capacity provided by the JBDPA seismic evaluation standard gave a conservative estimate for all specimens. This suggests that the JBDPA seismic evaluation standard should be used for evaluating ultimate drift angle after strengthening of a building using the proposed method.

Table 3. Strength of compression column and deformation capacity

Specimen	Flexural Strength Q_{mu}(kN)	Shear Strength Q_{su}(kN)	Q_{su}/Q_{mu}	Drift Angle of Ultimate State (%)	
				Experimental	Calculated
No.1	162.4	119.0	0.73	1.35	0.4
No.2	171.7	124.1	0.72	0.92	0.4
No.2	123.5	136.8	1.11	4.15	1.38
No.4	145.4	150.0	1.03	1.64	0.88

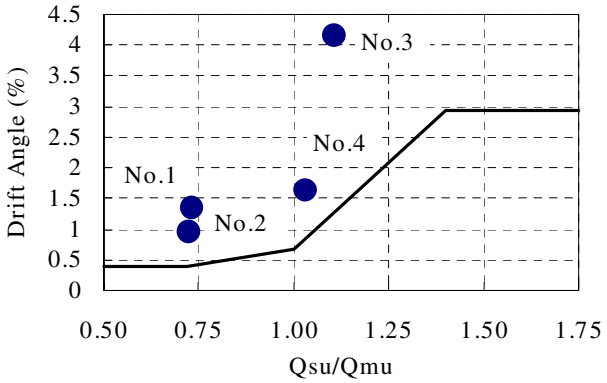

Fig. 7. Relationship between shear strength ration and deformation capacity

Deformation of the connecting beam

The lateral load-displacement relationship of the connecting beam that influenced structural performance after strengthening the frame is described. We [2, 3] tested the connecting beams under biaxial lateral load conditions with varying loading angles. Based on those experimental results, the load-displacement relationship was assumed in the analysis for the connecting beam, which are shown in Fig. 8. A multi-linear skeleton curve can be identified in the load-displacement curve. Three strengths were obtained: crack strength, yielded strength in normal reinforcing bars, and flexural strength. K is elastic stiffness up to cracking. K2 is the second modulus between post-cracking and normal reinforcement yielding. K3 is the third modulus between post-normal reinforcement yielding and flexural strength. K4 is the fourth modulus after flexural strength. The elasticity stiffness K in the direction of the deformation is shown assuming each elasticity modulus, K_x and K_y, in the X and Y directions as expressed in Eq. (3).

$$K = \sqrt{\left\{(\cos\theta / K_y)^2 + (\sin\theta / K_x)^2\right\}} \tag{3}$$

$$K_i = 1/\left(1/K_{bi} + 1/K_{si}\right) \tag{4}$$

Where θ, k_{bi}, k_{si} is the angle of the brace in the horizontal direction, the flexural stiffness, the shear stiffness.

Decreasing stiffness factor α_y at the yield strength to use for the calculation of K2 is given by

$$\alpha_y = \left\{0.043 + 1.65\left[n_0 p_{t0} + n_s\left(\sigma_{sy}/\sigma_{sy0}\right)P_{gs}\left(d_{gs}/D\right)\right] + 0.043(a/D)\right\}(d_0/D)^2 \tag{5}$$

Where n_0 is the modular ratio of normal-strength reinforcement, p_{t0} is the tension reinforcement ratio of normal-strength reinforcement, n_s is the modular ratio of high-strength rod, σ_{sy}, σ_{sy0} are the yield stress of normal-strength reinforcement and high-strength rod, respectively, p_{gs} is the tension reinforcement ratio of high-strength rod, d_{gs} is the length between the extreme compression fiber and center of prestressing force, D is the depth, a/D is shear span ratio, d_0 is effective depth of tension reinforcement. The decreasing stiffness factor α_y was proposed by Hamahara et al. [4].

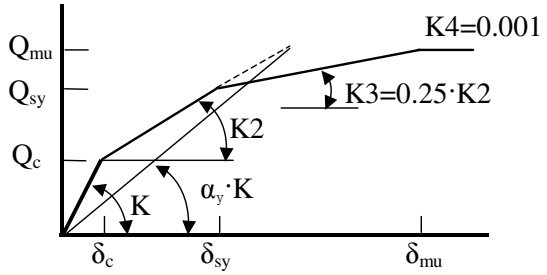

Fig. 8. Skeleton model of lateral load-displacement relationship for connecting beam

The formula for strength interaction in calculating flexural crack strength was assumed to be a straight line, and the formula in the calculation of flexural strength in normal reinforcing bars yielded and ultimate flexural strength was assumed to be an ellipse.

The flexural crack strength M_c is given by

$$\left(M_c\cos\theta / M_{cx}\right) + \left(M_c\sin\theta / M_{cy}\right) = 1 \tag{6}$$

$$M_{ci} = (0.07F_c + \sigma_0)Z_{ei} \tag{7}$$

Where M_{ci} are flexural crack strength in the X and Y directions and Z_{ei} is the effective section modulus. Here, M_{ci} is given in the AIJ Standard [5].

The flexural strength M_{sy} for normal reinforcing bars yielded is given by

$$\left(M_{sy}\cos\theta / M_{syx}\right)^2 + \left(M_{sy}\sin\theta / M_{syy}\right)^2 = 1 \tag{8}$$

$$M_{syi} = 7/8 \cdot d_{0i} \cdot A_{soi} \cdot \sigma_t + P_n(d_p - d/8) \tag{9}$$

Where d_{0i}, A_{s0i}, σ_t is the effective depth for tension reinforcement, sectional area of reinforcement, the yield strength, respectively, for normal-strength reinforcement. P_n is the effective prestressing force and d_p is the effective depth for all high strength rods. Here, M_{syi} is given in the AIJ Recommendations [6].

The ultimate strength M_u is given by

$$\left(M_u\cos\theta / M_{ux}\right)^2 + \left(M_u\sin\theta / M_{uy}\right)^2 = 1 \tag{10}$$

$$M_{ui} = (d_i - k_0 X_{ni})A_{si}\sigma_{sy} + (d_{0i} - k_0 X_{ni})A_{s0i}\sigma_{sy0} \tag{11}$$

Where, X_{ni}, A_{si}, d_i is neutral axis depth, sectional area of high-strength rod, and effective depth for high-strength rod. K_0 is the coefficient of stress block, equal to 0.42. Here, M_{ui} is given in the AIJ Standard [5].

The load-deformation relations of the connecting beam on the upper compression side of the column are shown in Fig. 9 and 10. As the load is the component force in the X or Y direction of the brace axial force, deformation shows the relative displacement of the connecting beam in each principal direction based on the beam. The relative deformation of the connecting beam was measured by LVDT attached to an instrumentation frame, which was mounted on the original beam. The broken lines in the figure show the proposed load-deformation relations. The proposed model corresponds to the experimental results, indicating that its application to the design is possible.

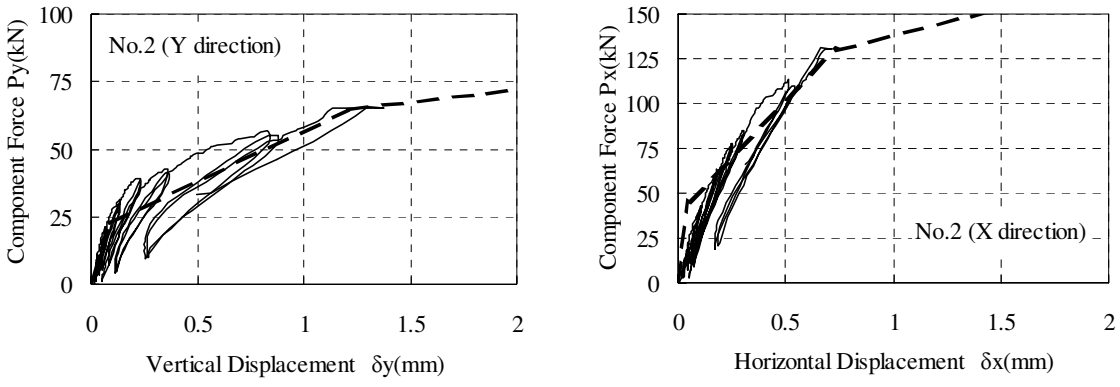

(a) No.2 (in Y Direction) (b) No.2 (in X Direction)

Fig. 9. Load-displacement responses of connecting beam

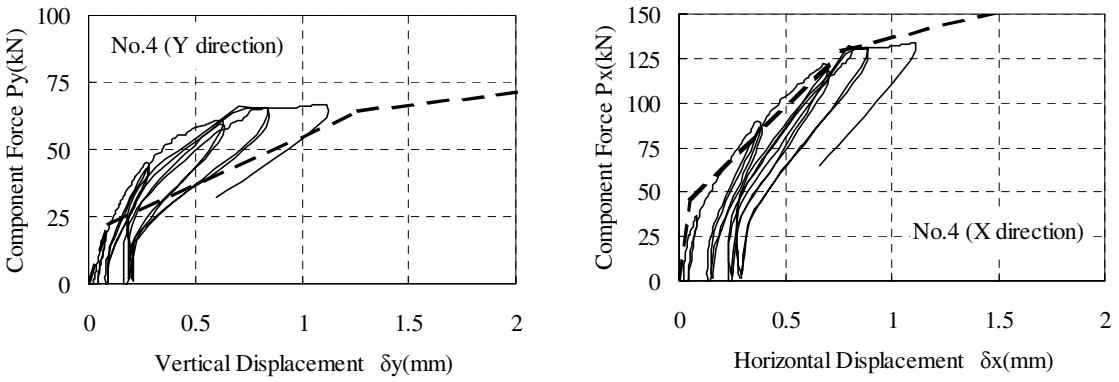

(a) No.4 (in Y Direction) (b) No.4 (in X Direction)

Fig. 10. Load-displacement responses of connecting beam

Drift angle in the brace yield

The relations between the brace axial load and drift angle of the frame is important in the strengthening design, it is described. Figure 11 shows the deformation of the original frame and connecting beam. Based on geometrical relations in consideration of the deformation of a connecting beam, the relationship between the drift angle and lateral load are given by Eq. (12).

$$\delta = \frac{LP}{E_b A_b \cos^2\theta} + (\delta_x + \tan\theta \cdot \delta_y) \tag{12}$$

Where L, P, E_b, A_b is the span, lateral load, Young's modulus of the brace, sectional area of brace. δ_x and δ_y are displacement of the connecting beam in the X and Y directions, given by the proposed skeleton model of the load-displacement relationship for the connecting beam.

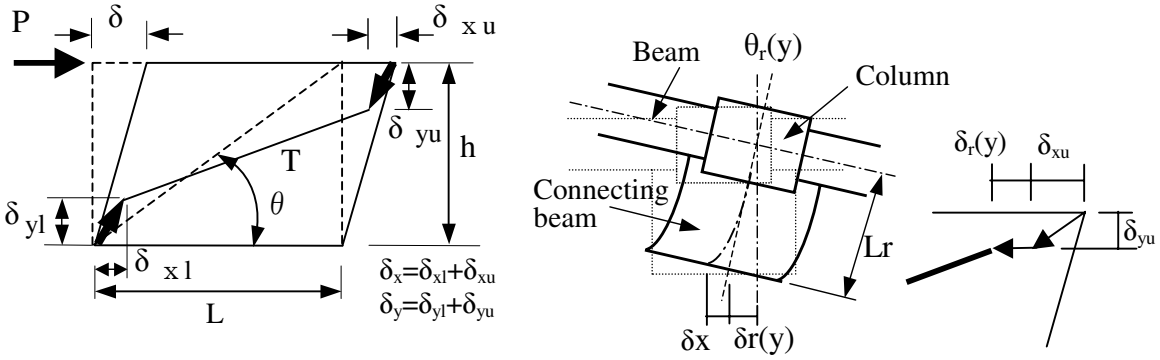

(a) Frame (b) Added deformation of the connecting beam due to the rotation

Fig. 11. Schematic illustration of deformation

There is no floor with beams, and all specimens had only one frame. For these reasons, the rotational stiffness around the Y-axis of the column-beam joint resulting from the connecting beam cast on the specimen is small in comparison with the actual size of the building. Because of this, additional deformation of the connecting beam developed due to the rotation of the X- and Y-axis of the column-

beam joint. Eq. (12) takes into consideration the added deformation. The influence of the additional displacement in the Y direction due to the rotation of the X-axis is ignored because it is small. However, taking into consideration the added deformation of the connecting beam due to the rotation of the X- and Y-axis, Eq. (12) is revised as follows:

$$\delta = \frac{LP}{E_b A_b \cos^2 \theta} + (\delta_x + \delta_r(y) + \tan\theta \cdot \delta_y) \tag{13}$$

$$\delta_r(y) = \theta_r(y) \cdot L_r \tag{14}$$

Where L_r is the length of the connecting beam, θ_r (y) is the angle for Y rotation. δ_r (y) is X-direction displacement in Y rotation.

Figure 12 shows the relationship between the brace axial load and drift angle. A comparison of the experimental value and the calculation is provided in Table 4. The brace axial load was estimated using the average strain. Herein, the lateral displacement subtracting the additional deformation of the connecting beam due to the rotation of the Y-axis of the column-beam joint was used for the calculation of the drift angle.

The experimental results and calculation values show good correspondence with all specimens. The drift angle at yielding of the brace can be estimated with satisfactory precision. This suggests that it can be used for the strengthening design.

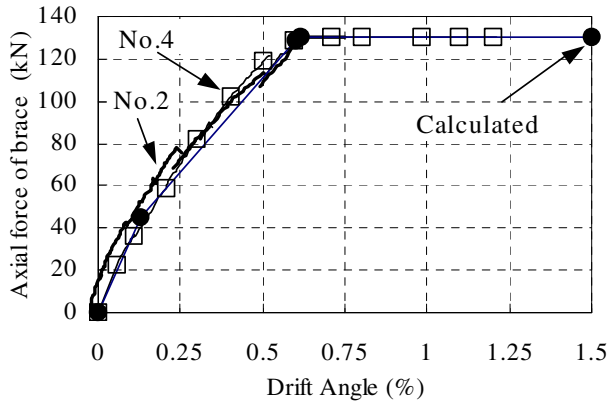

Fig. 12. Axial force/drift angle responses

Table 4. Drift angle in brace yield

Specimen	Experimental (%)	Calculated (%)
No.2	0.602	0.601
No.4	0.615	0.614

CONCLUSIONS

A new seismic strengthening method was developed using outer-frame braces. Seismic performance of the frame strengthened by attaching an outer-frame brace was investigated experimentally. Based on the experimental results reported herein, the following conclusions can be drawn:

1. Original and strengthened specimens exhibited responses up to the lateral load-carrying capacity with very similar lateral load displacement curves. This is seen in both shear and flexural failure type specimens. The strength of the frame after attaching the outer-frame is given as the sum of the strength of the frame and brace.
2. Deformation capacity of the specimens was evaluated using shear strength ratio according to the seismic evaluation standard. All experimental deformation capacity results were greater than that given by

the JBDPA seismic evaluation standard. The seismic evaluation standard should be used for evaluating the ultimate drift angle after strengthening the building using the proposed method.
3. The lateral load-displacement relationship of the connecting beam, which influenced structural performance after strengthening the frame, was proposed. The load-displacement relationship is based on the results of loading tests conducted on the connecting beam. It is possible to evaluate the drift angle at yielding of the brace by using the proposed load-deformation curve of the connecting beam.

ACKNOWLEDGMENTS

A new seismic strengthening method using outer-frame braces was developed under the technical affiliation between HAZAMA Corporation and SEIBU Construction Co., Ltd.

REFERENCES

1. Japan Building Disaster Prevention Association, “Seismic Evaluation Standard for Existing Reinforced Concrete Buildings”, *Japan Building Disaster Prevention Association*, 2001 (in Japanese)
2. Matsuura, T. and Sumi, K. “Experimental study on seismic strengthening method using brace of outer-frame”, *Proceedings of the Japan Concrete Institute*, Vol. 23, No. 1, 2001, pp. 1015-1020 (in Japanese)
3. Matsuura, T. Makita, T. and Sumi, K. et al. “A Study on Seismic Strengthening Method Using Braces of Outer-Frame”, *Summaries of Technical Papers of Annual Meeting Architectural Institute of Japan*, 2003, C-2, pp. 721-722 (in Japanese)
4. Hamahara, M. et al., “Elasto-Plastic Hysteretic Behavior of Prestressed concrete Beams”, *Journal of Structural and Construction Engineering*, No. 410, April, 1990, pp. 63-69 (in Japanese)
5. Architectural Institute of Japan, “Standard for Structural Design and Construction of Prestressed Concrete Structures”, *Architectural Institute of Japan*, 1989 (in Japanese)
6. Architectural Institute of Japan, “Recommendations for Design and Construction of Partially Prestressed Concrete (Class III of Prestressed Concrete) Structures”, *Architectural Institute of Japan*, 2003 (in Japanese)